*Journal of Extracellular Biology*

RESEARCH ARTICLE OPEN ACCESS

# Separation Methods Affect Glycan Patterns in Extracellular Vesicle Preparations From Canine Osteoblasts and Osteosarcoma Cells

Daniela Cortes Galvez[1] | Silvio Kau-Strebinger[1] | Simone Gabner[1] | Ingrid Walter[1,2]

[1]Department of Biomedical Sciences and Pathobiology, Institute of Morphology, University of Veterinary Medicine Vienna, Vienna, Austria | [2]VetCore Facility for Research, University of Veterinary Medicine, Vienna, Austria

**Correspondence:** Daniela Cortes Galvez (daniela.cortes@vetmeduni.ac.at)

**Received:** 24 September 2025 | **Revised:** 8 January 2026 | **Accepted:** 22 January 2026

**Keywords:** bone tumor | ectosome | exosome | glycosylation | precipitation | size exclusion chromatography | ultracentrifugation

## ABSTRACT

Extracellular vesicles (EVs) are nanosized, membrane-enclosed particles released by cells, facilitating intercellular communication via the transfer of bioactive molecules from producing to recipient cells. EVs are involved in several physiological and pathological processes, including cancer progression. The glycosylation of EVs influences the attachment and uptake by recipient cells, among other processes. In this study, we investigated the glycan profile of EVs from canine osteosarcoma (OS) cells and non-cancerous canine osteoblasts in vitro, using lectin blots, following EV separation with ultracentrifugation (UC), size exclusion chromatography (SEC), and a commercial precipitation kit (TEI). Beyond phenotypic differences, purity and yield, separation methods led to heterogeneous protein glycosylation patterns of EV preparations, with the least reproducibility in TEI preparations. In cellular comparison, SEC revealed contrasting results, most consistently showing higher levels of specific sugars in EVs from canine osteoblasts, including the detection of a unique glycoprotein absent in UC and TEI preparations. Osteosarcoma cells and their EVs exhibited a relative reduction of glycoproteins compared to osteoblasts and their EVs. Additionally, specific sugars were more abundant in EV preparations relative to their corresponding cell lysates. In conclusion, this study highlights the critical influence of separation methods on EV characteristics, leading to differing glycan patterns.

## 1 | Introduction

Osteosarcoma (OS) is the most common primary malignant bone tumor in both humans and dogs, and it typically has a poor prognosis (Egenvall et al. 2007; Mirabello et al. 2009). Given its high metastatic rate, early detection is crucial for improving outcomes. A better characterization and understanding of OS biology and its molecular mechanisms are essential prerequisites for developing new diagnostic and therapeutic strategies. Osteosarcoma is defined by the WHO as an osteoid-producing tumor of mesodermal origin (Choi et al. 2021). The tumor can be primarily lytic, productive, or a combination of both. Its histological appearance is heterogeneous and dominated by pleomorphisms. There are various subtypes, depending on the location within the bone and the cell type of origin. The osteoblastic form is the most common subtype both in humans and dogs (Klein and Siegal 2006). Osteosarcomas are often high-grade tumors preferentially occurring at the metaphysis of limbal long bones. Due to its higher incidence and morphological and etiological similarities, canine OS serves as a model for studying the human disease (Fan and Khanna 2015). Therefore, canine OS studies are of high comparative relevance to humans (Pinho et al. 2012).

All cells, whether healthy or cancerous release extracellular vesicles (EVs) into the extracellular space (Mathieu et al. 2019). As a result, EVs are found in all body fluids (van Niel et al. 2018), but also in cell culture supernatants (Shekari et al. 2023), which renders them valuable for in vivo and in vitro studies, respectively. Formerly considered as cellular waste, EVs have arisen as an important means of cell-to-cell communication, delivering bioactive molecules from a producing cell to a recipient cell with the ability to modify the physiological and morphological state of the latter (Tkach et al. 2016). EVs have a unique composition depending on the producing cell, which alters under pathological conditions but is still representative for a specific diseased cell (Valadi et al. 2007).

EVs are nanosized particles surrounded by a lipid bilayer encapsulating a core that contains miRNAs, mRNAs, other noncoding RNAs, proteins, lipids, glycans, and metabolites in a specific composition that is determined by the producing cell (Lorencova et al. 2020). The main EV subtypes can be distinguished upon their biogenesis (Batista et al. 2011; van Niel et al. 2018). Exosomes are formed as intraluminal vesicles within multivesicular bodies (MVB) and released as exosomes as the MVB membrane fuses with the cell membrane (Badawy et al. 2019), ectosomes, or microvesicles, are generated by outward buddying of the cell membrane and (Bojar et al. 2022) apoptotic bodies are fragments of cells that underwent programmed cell death (Hauser et al. 2017). As the different EV isolation protocols do not allow to enrich exclusively one subtype, the terms "small EVs" and "large EVs" are recommended by the minimal information for studies of extracellular vesicles (MISEV) consortium (Welsh et al. 2024).

In recent years, the role of EVs in tumor development and progression has been extensively studied, revealing new opportunities for diagnosis, treatment, and prognosis of neoplastic diseases. EVs have been shown to play a key role in the formation of the pre-metastatic niche (reviewed by Costa-Silva et al. 2015; Pontis et al. 2023) by transforming the local and distant tumor microenvironment such as cancer-associated fibroblasts (Mazumdar et al. 2020). Hence, they might introduce new therapeutic avenues to inhibit tumor cell metastasis. Being easily accessible in fluids such as blood, saliva, and urine, EVs enable early detection of cancer as non-invasive liquid biopsies (Hoshino et al. 2020) and offer higher specificity and sensitivity in cancer biomarker screening when compared to whole-body fluid screening (Kumar et al. 2024). For example, HSP70 assessed in EVs from blood of cancer patients reflected HSP70 in tumors (lung and breast) and correlated with disease status (Chanteloup et al. 2020). Analysis of prostate-specific antigen expression in plasma exosomes showed that it is well suited to discriminate between healthy patients and those with prostate disease (Logozzi et al. 2019).

As early as 2013, the presence of EVs in the microenvironment of OS in a mouse model was reported (Garimella et al. 2013). Since then, EVs from OS cells have mainly been studied for their role in tumor progression and metastasis. EVs from metastatic OS cells were able to increase the migration and invasiveness of non-malignant osteoblasts in vitro (Gong et al. 2018). Furthermore, OS cell-derived exosomes have been reported to promote the expression of angiogenic marker VEGF-A and to induce endothelial cell tube formation (Raimondi et al. 2020), thus promoting neovascularization processes that are a prerequisite for tumor growth and progression. OS seeds tumor cells mainly to the lung via the bloodstream (Bruland et al. 2005), but the reason for this specific localization and the mechanism behind it are not yet fully understood. EVs may be involved in this process, as EVs released from highly metastatic clones of OS cells have been shown to selectively concentrate in lung tissue where they prepare the pre-metastatic niche by establishing a chemotactic gradient to recruit OS cells (Macklin et al. 2016; Zhongyu et al. 2024) and alter the phenotype of low metastatic OS cells to highly metastatic (Macklin et al. 2016). Based on these reports, it is evident that EVs have a major impact on the metastatic behavior of OS tumor cells and that a profound knowledge of their molecular composition will help to elucidate the diagnostic, prognostic, and therapeutic potential.

The biodistribution of EVs, their attachment and uptake by recipient cells are far from being fully understood. Glycosylation is one of the most important post-translational modifications of proteins, for instance, facilitating their proper folding. In EVs, glycosylation has a high impact on their formation (Carnino et al. 2020), protein loading (Liang et al. 2014; Naito et al. 2021), attachment/biodistribution (Royo et al. 2019), and uptake by recipient cells (Christianson et al. 2013; Nishida-Aoki et al. 2020; Wang et al. 2020). The glycopattern of cancer cells and their released EVs show an aberrant glycosylation (Zhang et al. 2022), for example, a higher degree of sialylation and enrichment of complex *N*-glycans compared to non-cancerous cells (Escrevente et al. 2013). The glycocalyx on the exofacial side of EVs has a significant impact on their uptake by recipient cells. Removal of *N*- and *O*-glycosylation from EVs from breast cancer cell lines with different metastatic potential significantly stimulated uptake into blood endothelial cells (Nishida-Aoki et al. 2020). These results demonstrated that the EV glycosylation pattern, together with surface proteins, acts like a signature and prevents non-specific cellular uptake. High-content screening of the uptake behavior of deglycosylated varieties of EVs on a panel of cell lines yielded more distinct results, as different cell types preferred distinct glycosylation patterns (Williams et al. 2019). EV uptake also has an impact on the phenotype of tumor cells. It has been shown that the uptake of deglycosylated EVs by metastatic breast cancer cells significantly reduces their invasiveness in vitro (Menck et al. 2014), highlighting the role of the EV glycocalyx in the tumor metastatic process. Lectin microarray analysis of EVs from a panel of cell lines showed a conserved lectin binding pattern with enrichment in mannose, polylactosamine, $\alpha$-2,6 sialic acid, and complex N-linked glycans compared to the producing cells. However, they showed little to no binding to lectins that recognize terminal *N*-acetyl-D-galactosamine (CAA, DBA, SBA, SJA, and BPA) and blood group A/B sugar residues (Batista et al. 2011).

Data on the glycan features of OS cell-derived EVs are scarce for both humans and canines. It has recently been shown that different separation protocols yield EV populations with distinct glycan signatures, even when derived from the same human gastric cancer cell line, MKN45 (Freitas et al. 2019). Based on this, we anticipated that the choice of EV separation method would similarly shape protein glycosylation patterns in EVs from metastatic canine osteosarcoma cells (D-17) but also canine osteoblasts (CnOb). Three commonly used separation techniques—ultracentrifugation (UC), size exclusion chromatog-

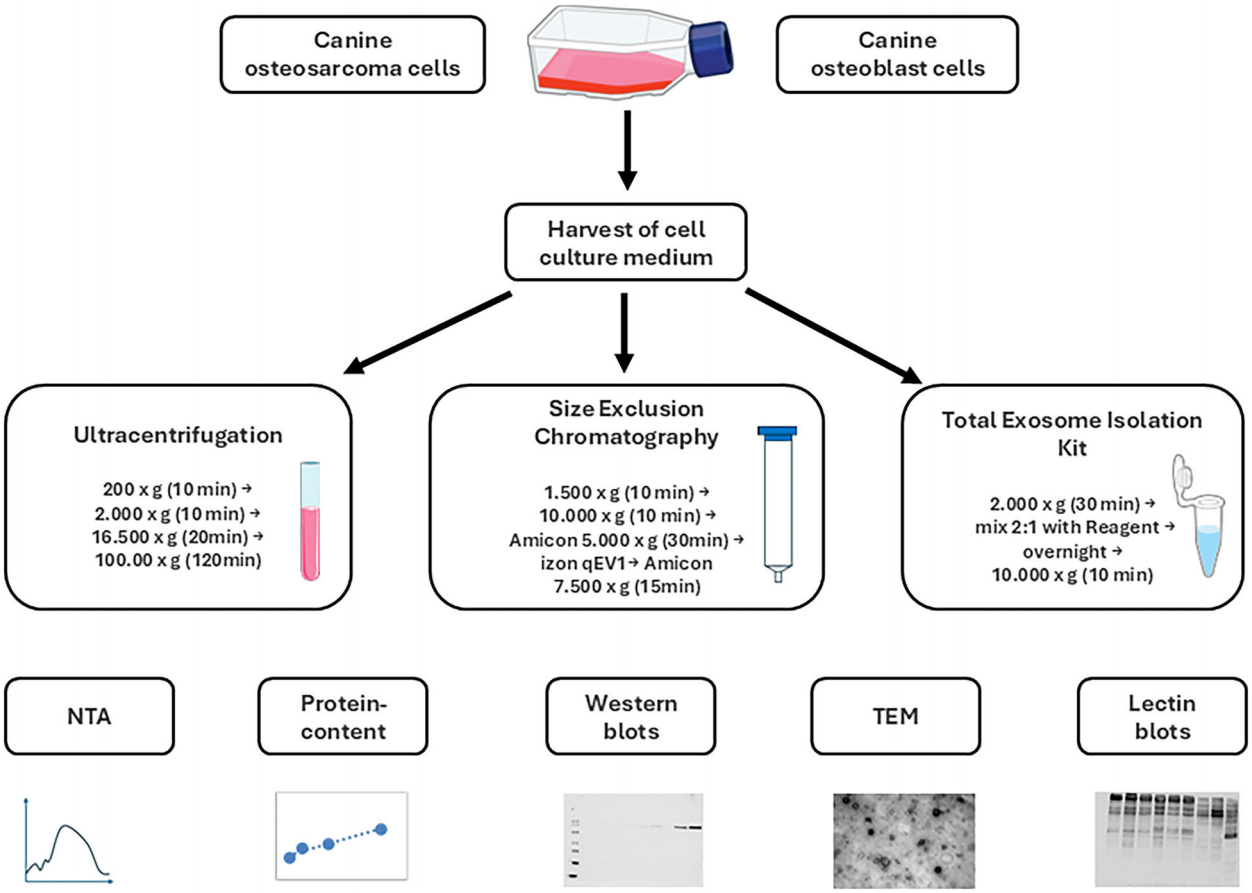


**FIGURE 1** | Schematic illustration of workflow with extracellular vesicle (EV) separation protocols, EV characterization, and glycan analysis.

raphy (SEC), and the Total Exosome Isolation (TEI) precipitation kit—were tested. Within each separation method, we further compared glycosylation patterns of EVs across cell types to identify disease-relevant glycan signatures and examined protein glycosylation differences between cells and their released EVs.

## 2 | Materials and Methods

### 2.1 | EV-Track

We employed the EV-TRACK platform (Van Deun et al. 2017) to ensure comprehensive and transparent reporting of EV experiments performed. Our study was assigned the EV-TRACK ID EV250082. The calculated EV-METRIC, reflecting the percentage of fulfilled components from the EV-TRACK checklist for individual experiments can be found under this ID. Figure 1 provides a summary of the experimental workflow, offering an overview of the steps involved in our EV experiments and facilitates determination of the EV-METRIC. The following sections detail specific methods, procedures, and materials used. MISEV guidelines (Welsh et al. 2024) were followed to the extent feasible.

### 2.2 | Cell Culture

Canine D-17 osteosarcoma cells (CCL-183, ATCC, Manassas, VA, USA) and canine osteoblasts (CnOb) (CN406-05, Sigma-Aldrich, St. Louis, MO, USA) were used in the present study. Both cell lines were cultivated in MEM Eagle medium (P04-08050, PAN Biotech, Aidenbach, Germany) supplemented with 10% fetal calf serum (FCS) (P30-3302 PAN Biotech), 1% L-glutamine (X0551, Biowest, Nuaillé, France), and 1% penicillin–streptomycin–amphotericin B solution (A5955, Sigma-Aldrich) at 37°C and 5% $CO_2$. D-17 and CnOb cells were seeded in T75 flasks (Sarstedt, Nümbrecht, Germany) at a density of $1.33 \times 10^4/cm^2$ ($=1 \times 10^6$/flask) and $2.66 \times 10^4/cm^2$ ($=2 \times 10^6$/flask), respectively. After 5 days of expansion, confluent cells were washed three times with PBS (D8662, Sigma-Aldrich) and the medium was changed to serum-free growth medium for 48 h. Conditioned medium was then removed and subjected to different EV separation protocols.

To assess the number of live and dead cells per flask after 48 h without FCS, supernatant and adhered cells were analyzed. Cells were detached using trypsin, stained with trypan blue and analyzed by an automated cell counter (Cell Countess 3, Invitrogen, Carlsbad, California, USA).

For western blotting and lectin blotting, the cells were washed with PBS, removed from the flask using a cell scraper and centrifuged at 5000× *g*. After removing PBS, the dry pellet was lysed with RIPA buffer (50 mM Tris–HCl pH 7.4, 500 mM NaCl, 0.5% sodium deoxycholate (all Carl Roth GmbH, Karlsruhe, Germany), 1% Nonidet P-40 (Igepal, Sigma-Aldrich), 0.1% sodium dodecyl sulfate (Serva, Mannheim, Germany)) supplemented with 1% protease and phosphatase inhibitors (Protease Inhibitor Cocktail and Phosphatase Inhibitor Cocktail 3, P8340 and P0044; both Sigma-Aldrich).

## 2.3 | Separation of EVs

### 2.3.1 | Differential Centrifugation/UC

Conditioned medium of D-17 and CnOb cells (70 mL each) was collected and centrifuged at 300× *g* for 10 min. The resulting supernatant (SN) was then centrifuged at 2000× *g* for 10 min. Subsequently, the SN was subjected to another centrifugation step at 16,500× *g* for 20 min. Differential centrifugation was performed at 4°C using a 5430R tabletop centrifuge equipped with a F 35-6-30 rotor (Eppendorf, Hamburg, Germany). Cleared SN was further passed through a 0.22 µm pore filter unit (Filtropur, Sarstedt) into 13 mL open top polyallomer centrifugation tubes (5030, Seton, Petaluma, California) and ultracentrifuged using a swing-out bucket rotor (SW41Ti) and an Optima LE 80K ultracentrifuge (Beckman Coulter, Brea, California, USA) at 100,000× *g* and 4°C for 120 min (k-factor: 124). The SN was discarded, and the pellets were resuspended in freshly filtered PBS by Filtropur 0.22 µm pore filter unit (for NTA and drop on grid) or in RIPA buffer (for western blot and lectin blot analysis) and stored at −80°C until further analysis. For transmission electron microscopy of ultrathin EV sections, EV pellets were fixed in 3% glutardialdehyde (Merck, Darmstadt, Germany) in Soerensen buffer.

### 2.3.2 | Differential Centrifugation/SEC

Conditioned medium of D-17 and CnOb cells (300 mL each) was collected and centrifuged at 1500× *g* for 10 min. The resulting SN was then centrifuged at 10,000× *g* for another 10 min, following the manufacturer's instructions. The cleared SN was transferred into 10 kDa MWCO ultrafiltration units (Amicon Ultra 15, UF 9010, Merck) and concentrated at 5000× *g* for 30 min. Differential centrifugation and concentration were performed at 4°C using the above specified centrifuge and rotor. The concentrate was loaded onto a qEV1 35 nm SEC column (izon, Christchurch, New Zealand); void volume: 2 mL, fraction volume: 0.7 mL. The SEC was performed according to manufacturer's instructions using an automatic fraction collector (izon). The column was pre-equilibrated with filtered PBS before sample application. Of the resulting fractions, fractions two, three, and four, which had shown the strongest CD81 signals in preliminary western blot analysis, were pooled, while the other fractions were discarded.

The pooled fractions were concentrated again using Amicon Ultra 15 ultrafiltration units to obtain a reasonable protein content for western and lectin blot analysis. Samples were stored at −80°C, or lysed with 8× RIPA buffer to avoid sample dilution and stored at −80°C. For transmission electron microscopy, pooled fractions were further ultracentrifuged at 100,000× *g* at 4°C for 90 min and the pellets were fixed in 3% glutardialdehyde.

### 2.3.3 | TEI Reagent

Conditioned medium of D-17 and CnOb cells (10 mL each) was collected and centrifuged at 2000× *g* for 30 min (according to manufacturer's instructions). The SN was mixed in a 2:1 ratio with TEI Reagent (4478359, Invitrogen) and incubated overnight at 4°C. The samples were then spun at 10,000× *g* for 60 min. All centrifugation steps were performed at 4°C using the above specified centrifuge and rotor. The remaining pellet containing the precipitated EVs was processed as described for UC.

## 2.4 | Nanoparticle Tracking Analysis (NTA)

Numbers and hydrodynamic diameter of enriched particles were measured using a ZetaView TWIN x20 system (Particle Metrix, Inning am Ammersee, Germany). The EV enriched samples were diluted in 0.22 µm filtered aqua bidest. to obtain 200–400 particles per frame. Measurements were performed in scatter mode with a 488 nm laser, sensitivity of 80, shutter speed of 100, minimum brightness threshold of 30, maximum brightness of 255, minimum area of 10 pixels, maximum area of 5000 pixels, bin size of 5 nm, and a fixed temperature of 23°C. Technical triplicates were conducted to ensure reproducibility. Data acquisition was performed using the ZetaView software version 8.06.01 SP1 (Particle Metrix). The obtained data were statistically analyzed and displayed using GraphPad Prism software version 10 (Dotmatics, Boston. USA).

## 2.5 | Western Blot Analysis

Protein content of EV lysates from D-17 and CnOb cells, and the corresponding whole cell lysates obtained by mechanically disrupting the cells prior to lysis was measured using the DC Protein Assay (5000116, BioRad, Hercules, CA, USA,) according to manufacturer's instructions and a Tecan Infinite 200 Pro plate reader (Tecan Life Sciences, Männedorf, Switzerland).

Lysates of EVs and cells were loaded with 3 µg protein per lane on 10% polyacrylamide gels using a Mini Protean Tetra System (BioRad). After electrophoresis at 200 mV, proteins were blotted onto a PVDF membrane (1620264, BioRad) using 350 mA for 60 min. The membranes were then blocked with 10% western blot blocking solution (11921673001, Roche Mannheim, Germany) in TBST for 2 h at room temperature to prevent unspecific antibody binding. Membranes were incubated with the respective primary antibodies (Table 1) at 4°C overnight in a tube rotator and subsequently washed in TBST five times for 8 min each. Afterward, membranes were incubated with HRP-conjugated secondary antibody (Table 1) for 30 min at room temperature, washed four times for 8 min each in TBST, followed by a final wash in TBS for 8 min. The chemiluminescence signal was detected using ECL Western Blot Detection Reagents (GE Healthcare, Chicago, IL, USA); a ChemiDoc Imaging System and Imaging Software version 6.0 (both BioRad).

## 2.6 | Lectin Blot Analysis

Lectin blots were performed following the western blot protocol as described with a loading amount of 3 µg total protein per lane. Loading was controlled on a Coomassie stained gel and evaluated by total lane volume assessment (BioRad Image Lab 6.0, Supplement 1a and b). After transfer to PVDF membranes,

**TABLE 1** | Antibodies.

| Antibody | Method | Clone | Dilution | Source | Catalogue number |
|---|---|---|---|---|---|
| a-CD81 | WB | JS81 | 1:1000 | BD Transduction Laboratories | 555675 |
| a-Flot1 | WB | D2V7J | 1:1000 | Cell Signaling | 18624 |
| a-ALIX | WB | 3A9 | 1:1000 | ABcam | Ab117600 |
| a-Calnexin | WB | | 1:2000 | Sigma-Aldrich | C4731 |
| a-Mouse-HRP | WB | | 1:1000 | Cytiva | NA931 |
| a-Rabbit-HRP | WB | | 1:1000 | Cytiva | NA934 |

**TABLE 2** | Lectins and corresponding sugars (Bojar et al. 2022).

| Lectins (biotinylated) | Catalogue number (all Vector Laboratories) | Corresponding sugar |
|---|---|---|
| Concanavalin A (**Con A**) | BK-1000 | A-Mannose (Man) |
| *Ricinus communis* agglutinin (**RCA**) | BK-1000 | Terminal *N*-acetyl-lactosamine (LacNAc), galactose (Gal) |
| Wheat germ agglutinin (**WGA**) | BK-1000 | Terminal *N*-acetyl-glucosamin (GlcNAc) |
| *Griffonia simplicifolia* Lectin I (**GSL I**) | BK-2100 | Terminal $\alpha$ galactose (Gal), *N*-acetyl-galactosamine (GalNAc) |
| *Lens culinaris* agglutinin (**LCA**) | BK-2100 | Core fucose (Fuc), $\alpha$-mannose (Man), |
| *Pisum sativum* agglutinin (**PSA**) | BK-2100 | Core fucose (Fuc), mannose (Man) |
| *Phaseolus vulgaris* erythroagglutinin (**PHA-E**) | BK-2100 | Complex N glycan epitopes, bisecting GlcNAc |
| *Erythrina cristagalli* lectin (**ECL**) | BK-3000 | *N*-acetyl-galactose (GalNAc), galactose (Gal) |
| *Datura stramonium* lectin (**DSL**) | BK-3000 | *N*-acetyl-glucosamine (GlcNAc) |
| *Griffonia simplicifolia* Lectin II (**GSL II**) | BK-3000 | *N*-acetyl-glucosamine (GlcNAc) |
| *Sambucus nigra* lectin (**SNA**) | B-1305-2 | Sialic acid (Sia) |
| *Maackia amurensis* Lectin I (**MAL I**) | B-1315-2 | Sialic acid (Sia), galactose on *N*-acetyl-lactose |

these were blocked in 2% bovine serum albumin (BSA) (8076.2, Carl Roth) dissolved in TBST and then incubated with respective biotinylated lectins (Table 2) at a concentration of 2 mg/mL in 1% BSA in TBST. After overnight incubation at 4°C, membranes were washed in TBST as mentioned above. Membranes were then incubated for 30 min at room temperature with HRP-conjugated Streptavidin (SA-5014, Vector Laboratories, Newark, California, USA) to detect bound biotinylated lectins. Membranes were washed, and the signal was detected according to the protocol for western blots.

After imaging, the total lane volumes of every lectin blot were calculated in arbitrary units using the Image Lab software version 6.0 (BioRad). Briefly, the whole cell lysates of CnOb und D-17 were analyzed and depicted. The calculated mean values of the EVs compared to the value of their producing cell was depicted for CnOb and D-17. The values of the triplicates of every EV separation method were demonstrated separately for all applied lectins and compared for CnOb and D-17 preparations.

## 2.7 | Transmission Electron Microscopy (TEM)

### 2.7.1 | Drop on Grid, Negative Staining

Ten microliters of EV samples (pellets suspended in filtered PBS) were dropped on 300 mesh formvar/carbon hexagonal copper grids (FCF300H-CU-SB, Science Services, Munich, Germany) and incubated for 1 h at room temperature. Remaining liquid was removed, and the grid was washed in three drops of aqua bidest. consecutively for 10 min each. Then the samples were fixed in 1% glutardialdeyhde (Merck) in Soerensen phosphate buffer for 5 min and washed with aqua bidest. before contrast enhancement with 2% aqueous uranyl acetate (Fluka Chemie AG, Buchs, Switzerland). After negative staining, remaining liquid was removed with a filter paper. The air-dried grids were analyzed with a transmission electron microscope (EM 900, Zeiss, Oberkochen, Germany) equipped with a slow-scan CCD camera (2K Wide-angle Dual Speed, TRS, Moorenweis, Germany) and ImageSP Professional software version 1.2.11.15 (TRS).

### 2.7.2 | Ultrathin Sections

EV pellets were fixed in 3% glutardialdehyde in Soerensen buffer and washed in Soerensen buffer prior to epoxy resin embedding. After postfixation for 2 h at room temperature in 1% osmium tetroxide (Electron Microscopy Sciences, Hatfield, PA, USA) and dehydration in an ethanol series (70%, 80%, 96%, and 100%) and an increasing series of propylene oxide (Sigma-Aldrich), pellets were embedded and polymerized in situ in epoxy resin (Serva) for 48 h at 60°C. Ultrathin sections (70 nm) were prepared and contrasted in methanolic uranyl acetate (Fluka Chemie AG) and alkaline lead citrate (Merck). The sections were analyzed using TEM and software as mentioned above.

## 2.8 | Statistical Analysis

All experiments were carried out at least in triplicates. Data outliers were identified wherever applicable and excluded using the ROUT method with a $Q$ value of 1%. Data was then assessed for normal distribution using the D'Agostino & Pearson test. Based on the results, appropriate parametric or non-parametric tests were selected. Tests used and sample sizes are mentioned in respective figure captions. Statistical significance was set at $p < 0.05$. Data analysis was performed in GraphPad Prism, version 10.4.1.

# 3 | Results

## 3.1 | EV Separation Method and Cell Type Influence the Quantitative and Qualitative EV Phenotype

To characterize nanoparticles in EV preparations from D-17 and CnOb conditioned cell culture medium using different EV separation methods, that is, UC, SEC, and TEI, we analyzed the particle concentration, size, structural features, protein content, and immunophenotype (Figure 1).

Despite both cell lines reaching confluency at the time of serum removal, the relative number of viable cells at time of harvest was significantly higher in D-17 cells with a mean of $8.8 \times 10^6$ and $3.64 \times 10^6$ for CnOb per flask (Figure 2a, Supporting Information) and a mean viability of 93% for D-17 and 68% for CnOb. In parallel, the number of particles per milliliter of conditioned medium was higher in D-17 preparations than in CnOb with a significant difference in TEI (Figure 2b). However, when normalizing the number of particles to the number of viable cells, there is a shift to more particles enriched per cell in CnOb UC and SEC preparations with a significant difference after SEC separation protocols (Figure 2c). Despite this observation, TEI preparations trended in opposite direction, but without resulting in a significant difference of particles per milliliter conditioned medium between D-17 and CnOb. NTA measurements revealed a median hydrodynamic diameter (±median absolute deviation) of particles in EV preparations from D-17 cells of 110.1 nm (±32.3 nm) for UC, 126.8 nm (±36.4 nm) for SEC, and 162.9 nm (±51.5 nm) for TEI, with significant difference between UC and TEI (Figure 2d). Particles from CnOb had median values of 149.0 nm (±37.3 nm) for UC, 154.0 nm (±46.4 nm) for SEC, and 161 nm (±50.6 nm) for TEI preparation, with no significant differences between separation methods (Figure 2d). Although separation with UC and SEC resulted in larger particles obtained from CnOb compared to D-17 cells, these differences were above the significance threshold (UC, $p = 0.060$; SEC, $p = 0.103$; TEI, $p = 0.655$).

Negative staining of separated particles prepared as drop on grid samples for TEM revealed presence of cup-shaped structures, mostly within the sub-200 nm size range (small EVs), across all applied methods (Figure 2e). D-17 3EVs from TEI preparations showed a higher tendency to form aggregates with electron dense material. Ultrathin sections of epoxy resin-embedded EV preparation pellets contained EVs of various shapes and sizes, surrounded by a bilayer membrane and a core with differing density in UC preparations of both cell types and SEC preparation of D-17 cells. SEC enriched CnOb particles and particles obtained by the TEI method were dense, homogenous and exhibited dark, round shaped structures with a textured surface and no clearly visible bilayer (Figure 2e).

The protein concentration of RIPA lysed EV preparations, normalized to 1 mL conditioned medium, was highest after TEI with a mean of 12.7 µg for D-17 and 11.3 µg for CnOb preparations. After UC the mean concentration was 4.0 µg for D-17 and 1.3 µg for CnOb-derived samples. SEC preparations led to the lowest protein concentration with a mean of 1.0 µg for D-17 and 0.7 µg for CnOb-derived samples. Differences were significant in D-17 preparations between UC and SEC and UC and TEI (Figure 2f). Normalizing the measured protein concentration to the mean particle number, the average protein concentration was 13 femtogram (fg) for D-17 and 5.5 fg for CnOb after UC, and 4.0 fg for D-17 and 3.4 fg for CnOb in SEC preparations. EV preparations using TEI led to markedly higher protein concentrations per particle, with 200 fg for CnOb (Figure 2g).

Western blot analysis revealed positive signals for the multipass transmembrane protein CD81 (tetraspanin) and the cytosolic protein ALIX for EV preparations using UC and SEC of D-17 and CnOb, while no signals were found after TEI except a weak CD81 band in D-17 EVs (Figure 2h). CD81 and ALIX were almost absent in whole cell lysates. Flotillin-1, a caveolae-associated membrane protein, was present in all EV preparations and cell lysates, with the weakest band observed in D-17 EV preparations using TEI. Calnexin, an endoplasmatic reticulum marker, showed strong signals in cell lysates and in EV preparations from CnOb using TEI but was weak or absent in all other samples (Figure 2h).

## 3.2 | Glycan Patterns in EV Preparations are Highly Influenced by the Separation Method and Cell Type

Lysates of EVs released by D-17 and CnOb cells, and the respective whole cell lysates were analyzed by lectin blotting. Twelve lectins with binding affinities to the most common sugar residues were used to detect the corresponding sugars on glycoproteins. Generally, EVs enriched by UC and SEC resulted in more reproducible glycan patterns within the triplicates compared to the TEI preparations. EVs predominantly showed glycosylation

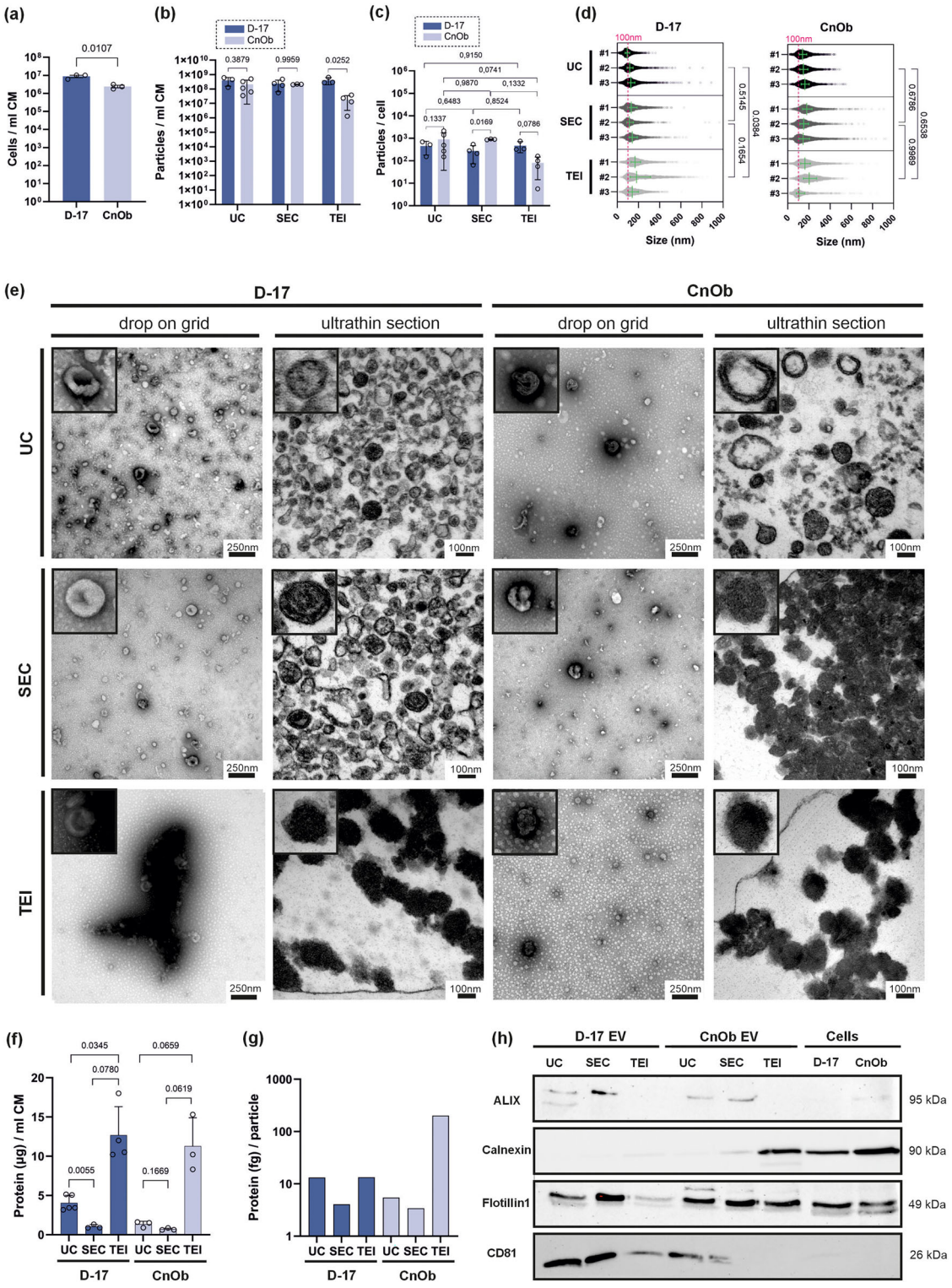


**FIGURE 2** | Characterization of EVs released by canine osteosarcoma cell line (D-17) and canine osteoblasts (CnOb), isolated by ultracentrifugation (UC), size exclusion chromatography (SEC), and total exosome isolation kit (TEI). (a) Number of living cells at the harvesting time per milliliter of cell culture medium. *p*-Values calculated after unpaired Student's *t*-test. (b) Number of measured particles per milliliter of conditioned medium, comparing EVs from D-17 and CnOb cells and UC, SEC, and TEI as isolation methods. Two-way ANOVA was performed from a minimum of three replicates per isolation. (c) Number of particles normalized to the number of living cells per milliliter of medium, calculated for all isolation methods. Mixed-effect analysis with Tukey's multiple comparisons. (a–c) Dots represent independent cell culture replicates. (d) Particle diameter of minimum three replicates per method with the following medians for D-17: 110.1 nm (UC), 126.8 nm (SEC), and 162.9 nm (TEI). The medians for CnOb particles were 149.0 nm (UC), 154.0 nm (SEC), and 161.4 nm (TEI). The adjusted *p*-values after nested one-way ANOVA are indicated on the right side. (e) Transmission electron microscopy (TEM) images of different preparations with negative staining of drop-on-grid method on the left side and ultrathin sections of Epon-embedded EV pellets on the right side. At the top left of every image the close-up shows single particles, cup shaped in the drop-on-grid preparations

and round to spherical, sometimes with a visible surrounding double membrane in the ultrathin sections. (f) Protein content per milliliter of conditioned medium in dependence of the cell of origin and the applied isolation protocols as determined by DC Protein Assay and a Tecan Infinite 200 Pro plate reader. *p*-Values calculated after mixed effect analysis. (g) Protein content normalized to the mean number of particles measured by NTA after the different isolation protocols. (h) Western blot of the EV markers ALIX, Flotillin 1, and CD81 and Calnexin as a cytoplasmic marker. EV preparations of different isolation protocols (UC, SEC, and TEI) and whole cell lysates were analyzed.

of large proteins at the size range of 260 kDa and beyond when compared to the respective cells (Figure 3).

Probing of neuraminic acid (sialic acid) resulted in different band pattern when comparing MAL I ($\alpha$2,3 sialylated LacNAc) and SNA ($\alpha$2,6 sialylated LacNAc) lectins. MAL I binding revealed glycoproteins mostly located between 70 and 140 kDa in EVs of D-17 and CnOb cells, a very faint signal at 45 kDa in the CnOb SEC preparation and glycoproteins with up to 260 kDa. In lysates of CnOb cells highly glycosylated proteins in size between 100 and 140 kDa were present, in D-17 cells, glycosylation was much lower.

After SNA lectin binding, proteins of multiple sizes were detected ranging from less than 25 kDa and below to large proteins in the range of 260 kDa and above, which were present only in the EV preparations but not in cell lysates. D-17 UC and SEC preparations revealed a similar glycosylation pattern with a moderately highlighted band of about 50 kDa and below 35 kDa in size. The 50 kDa band was also present in CnOb SEC EV lysates with a number of additional bands in larger size. Multiple protein bands were marked by SNA lectin blotting in both cell types, ranging from 25 to 140 kDa, with the strongest bands between 45 and 100 kDa.

Con A, a lectin predominantly binding $\alpha$-mannose sugar residues, detected multiple bands of glycoproteins in the range of below 25 to beyond 260 kDa with differences in band patterns between EVs originating from different cell types and differences between separation methods. Strong glycosylation was observed in very large proteins, which was in particular evident in D-17 EV preparations. In EVs of D-17 cells, a bold band of 37 kDa was detected after TEI and SEC separations but missing after UC, and a double band in CnOb EVs at 35–37 kDa was present among all separation methods. Prominent bands were observed between 40 and 50 kDa in CnOb SEC and TEI preparations. Both whole cell lysates revealed a wide variety of glycosylated proteins, with strong bands between 45 and 70 kDa that were also revealed in CnOb TEI preparations.

Blotting with the core fucose-binding (Fuc $\alpha$1-6) lectins PSA and LCA resulted in similar band patterns. Fucose glycosylation of large proteins (200 kDa and above) was detected in EVs from D-17 cells. In CnOb EVs, a range of different sized proteins (45–260 kDa) was seen in SEC preparations which were only faintly present or missing in UC and TEI preparations. Fucose-glycosylated proteins were scarce in the total cell lysates of CnOb and hardly noticeable in D-17.

The binding pattern of GSL I, a lectin specific for terminal $\alpha$-galactose, was quite similar in preparations of EVs of D-17 and CnOb with three bands of 260 kDa and above and a several bands at 100 kDa and higher, that were more evident in SEC and UC preparations and present also in cell lysates. The separation method had a minor impact on the binding pattern profile of this lectin, except a very strong band at 45 kDa and two fainter bands at 55 and 140 kDa that were detected only in SEC enriched EVs from CnOb.

Blotting with DSL for poly LacNAc on branched *N*-glycans resulted in a band pattern that was quite comparable between separation methods. DSL lectin bound proteins were mostly 100 kDa and above with a triple band visible in all preparations except in D-17 TEI, with a prominent band at 260 kDa in all CnOb preparations. In CnOb, a band at 60 kDa was present in UC and SEC preparations and an additional prominent band at 45 kDa only after SEC. UC preparations from both cell types showed a subtle signal between 40 and 50 kDa. WGA for terminal $\beta$ GlcNAc revealed marked glycoproteins that were generally larger than 100 kDa, except faint signals below in UC and SEC preparations and cell lysate of CnOb. A prominent band at 45 kDa was detected in CnOb after SEC. Signals above 260 kDa were present in all EV preparations except D-17 SEC and were the only detected signal in D-17 TEI. WGA binding revealed an evident difference in glycosylation after SEC separation with the highest abundance in CnOb and the weakest in D-17 preparations. GSL II (also binding terminal $\beta$ GlcNAc) marked glycoproteins above 260 kDa in EV preparations except D-17 SEC. Several smaller faint bands were present and similar in D-17 UC and SEC. A band of 37 kDa size was evident in all D-17 EV preparations and visible as a double band in CnOb EVs. Another double band at 120–140 kDa was detected in UC and SEC preparations of CnOb and fainter in D-17. The results of DSL and WGA blotting of the whole cell lysates revealed glycosylated proteins mainly between 100 and 140 kDa, whereas GSL II showed various glycosylated proteins in the size range of 35–140 kDa.

Lectin blotting with ECL to demonstrate binding of galactose/*N*-acetyl-galactosamine (GalNAc), showed a highly expressed band at about 45 kDa in CnOb EVs regardless of the separation method; in the UC preparation, the highlighted band was slightly larger. This band was very faint in CnOb cell lysates and not detected in D-17 EVs and D-17 cells. Additionally, a double signal at 260 kDa was present in both UC and TEI preparations, but more abundant in CnOb. In cell lysates, the bands were numerous and ranged from below 25 and 100 kDa.

Blotting with PHA-E lectin, which binds to complex *N*-glycan motifs (GlcNAc, LacNAc), showed differences between EV separation methods, most striking were bands between 40 and 50 kDa in EVs of CnOb after SEC. UC and TEI separation methods led to a higher amount of glycosylation above 260 kDA in both cell types but almost missing in SEC. The glycosylation pattern between 100 and 260 kDa was similar in CnOb but diverging in D-17 EVs. RCA I, which also binds to LacNAc, revealed glycosylation of large proteins in all EV preparations and a triple band at 110–140 kDa in CnOb EVs. The band at about 50 kDa was the most abundant

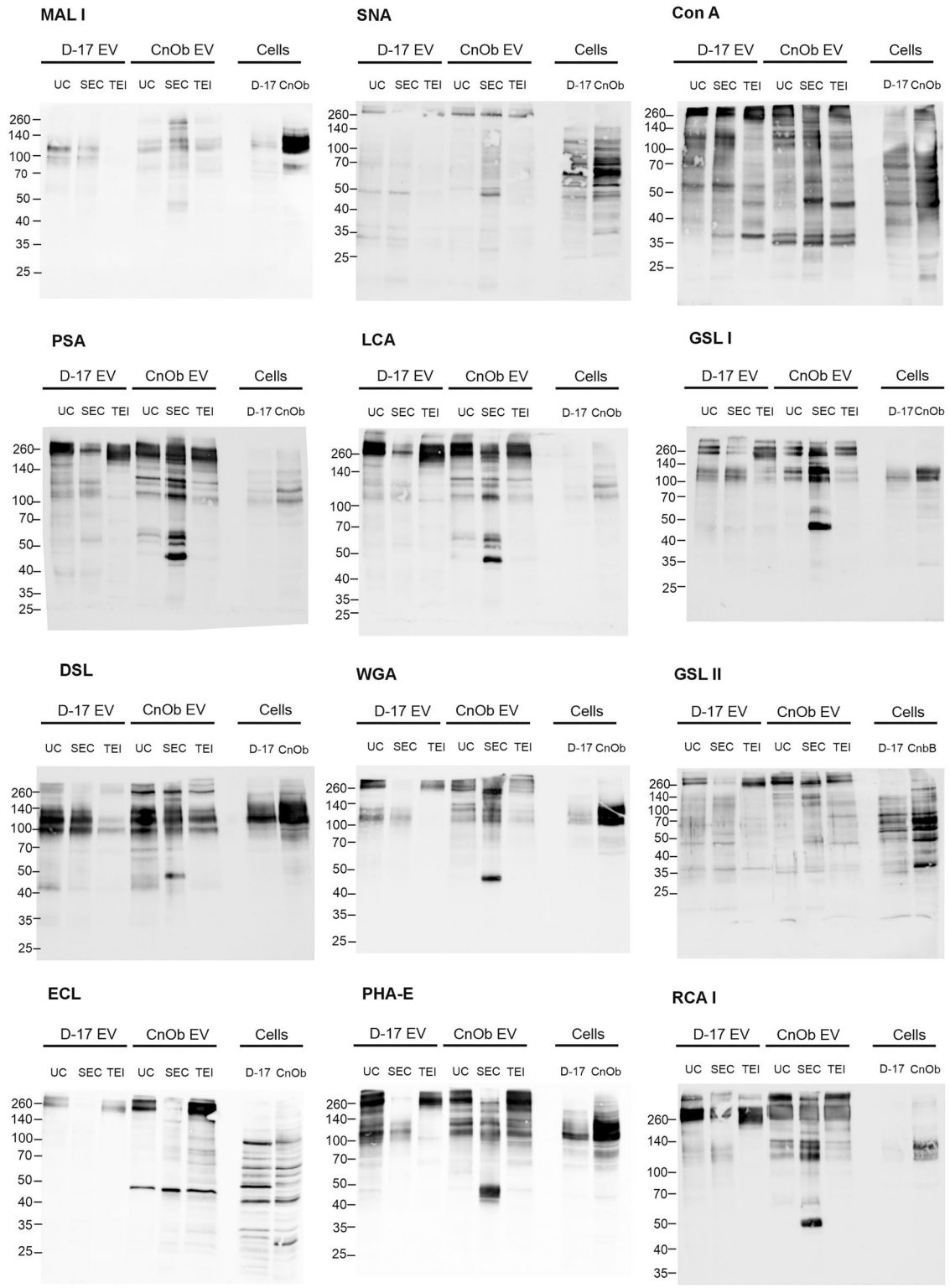


**FIGURE 3** | Lectin blotting of EV isolates from the canine osteosarcoma cell line (D-17) and canine osteoblasts (CnOb), isolated by ultracentrifugation (UC), size exclusion chromatography (SEC), and total exosome isolation kit (TEI), and the whole cell lysates from D-17 and CnOb cells. Three micrograms of protein per lane were applied, and the biotinylated lectins MAL I, SNA, Con A, PSA, LCA, GSL I, DSL, WGA, GSL II, ECL, PHA-E, and RCA I revealed the presence of the corresponding sugars.

of the additional lines present in CnOb SEC EVs. In whole cell lysates, RCA I and PHA-E blotting showed comparable result with a few bands at about 100 kDa, that were more prominent in the latter.

### 3.3 | Tumor Cells and Their EVs Show Reduced Glycosylation Compared to Non-Cancerous Counterparts

The comparison of the total lane volumes of lectin blots showed a lower degree of glycosylation of D-17 cells compared to CnOb in all 12 lectins analyzed (Figure 4a). When comparing the glycosylation of EVs to their cells of origin (Figure 4b,c), LCA binding sugars (Fuc $\alpha$1-6) had the highest abundance in EV preparations, followed by RCA I (LacNAc), PSA (also Fuc $\alpha$1-6). WGA, (GlcNAc), GSL I (Gal), and PHA-E (GlcNAc, LacNAc). MAL I and SNA (both sialic acids), GSL II (GlcNAc), and Con A (Man) were more abundant in the whole cell lysates than in EV preparations. The comparison of the total lane volumes of EV preparations with regards to the isolation methods (Figure 4d) resulted in a lower grade of glycosylation in D-17 EVs than in CnOb EVs, which was very pronounced with ECL binding to GalNAc. With most lectins, the lower glycosylation was more pronounced after SEC compared to TEI. The decrease of glycosylation in EVs of D-17 cells was less distinct after UC and some lectins (PSA, LCA, DSL, and PHA-E) even showed higher glycosylation in D-17 EVs after UC.

## 4 | Discussion

In this study, we demonstrated that EV separation methods exhibit a crucial effect on the protein glycosylation pattern detected in lectin blots. To our knowledge, this is the first study to report the composition of glycans in both canine metastatic OS cells (D-17) as well as CnOb cells and their EVs, suggesting a potential impact on the attachment and uptake by recipient cells and consequently metastatic tumor spread. While previous studies have focused on glycosylation changes in OS cells (reviewed by Di Gregorio et al. 2024), our findings extend this knowledge by showing that canine OS EVs also display altered glycosylation patterns compared to EVs of non-cancerous cells. Highlighting these differences might help to identify a tumor-specific EV population in the future.

Considering the total number of particles obtained from the same amount of conditioned medium, EV separation method had no significant influence in UC and SEC preparations. When normalizing the number of particles to the amount of viable cells, this resulted in more particles released per single cell in CnOb. This is somewhat contradictory to the literature, as cancer cells have been described to release a higher amount of EVs compared to non-cancerous cells (Jacobson et al. 2024). However, cultivation-related stress, for example, due to glucose or serum starvation, is a known factor enhancing EV release (Duan et al. 2024; Garcia et al. 2015), which was described in Jurkat T-cells, when serum in cell culture medium was reduced (Kao et al. 2023). In our setting, CnOb cells reacted more sensitive to serum removal as a stress factor compared to D-17 tumor cells, which is in accordance with other reports where serum deprivation was described to have no impact on cancer cell viability (Freitas et al. 2019).

In terms of EV size, the smallest particles from both cell types were obtained by UC preparations, followed by SEC, and TEI with the largest particles. As the recommended TEI isolation protocol lacks a previous high speed centrifugation step, larger particles like apoptotic bodies or debris might not be removed as effectively as by the other methods. This assumption was supported by TEM analysis and had been previously described for other cancer cell types (Freitas et al. 2019). Irrespective of the EV separation method used, the average median particle diameter was larger in CnOb compared to D-17 cells, which is probably the result of a different composition of the EV population released by non-cancerous and cancer cells as described before (Fan et al. 2020).

Analysis of the EV morphology by TEM drop on grid preparation showed cup-shaped forms, however, with a noticeable dark background in the D-17 TEI preparations, where EVs seemingly formed larger aggregates. In ultrathin sections of pelleted EVs, a clear bilayer lipid membrane was observed in UC isolations and SEC isolates of D-17 cells. TEI isolates from both cell types and SEC isolates from CnOb showed round electron dense structures lacking a bilayer membrane. The SEC results seem contradictory as the good performance in the other characterization pillars contrast with divergent TEM images. We speculate, that due to the tedious SEC processing, the CnOb EVs stability declined and made them more prone to shear forces in the UC pelleting step. Paul et al. (2022) demonstrated that colon cancer-derived EVs are enriched in surface hyaluronan compared to EVs from healthy cells, resulting in increased elasticity—hence higher mechanical resilience—as measured by atomic force microscopy. Accordingly, molecular alterations in the membrane of cancer EVs could make them more resistant to mechanical stress and thus could explain the observed differences in morphology between SEC EVs from D-17 and CnOb cells. The loss of functional proteins of the CnOb EV corona due to SEC separation that has been formerly described (Wolf et al. 2022) might also decline EV stability, leading to the altered morphology in TEM. Additional research is necessary to verify these assumptions.

The western blot results revealed a strong calnexin band in the TEI separation and a very faint band in the SEC CnOb EV preparation. Calnexin is not expected to be present in EVs, and we deduce that as CnOb reacted more sensitive to FCS deprivation, the reduced viability led to more cell debris in the preparations. Apparently, UC and to a lesser extend SEC were better suited to eliminate these particles.

UC and SEC isolates had CD81 bands of similar density, while it was faint in TEI preparations of D-17 and absent in CnOb. In this context, we want to point out again that we loaded the same total protein amount (3 µg/lane) for every sample, which does not represent the same number of particles. In TEI isolates, this protein amount was contributed by a considerably lower number of particles. Regarding the protein amount per particle observed with the other methods, we interpret the higher values in UC preparations as an indication of co-isolated proteins. These

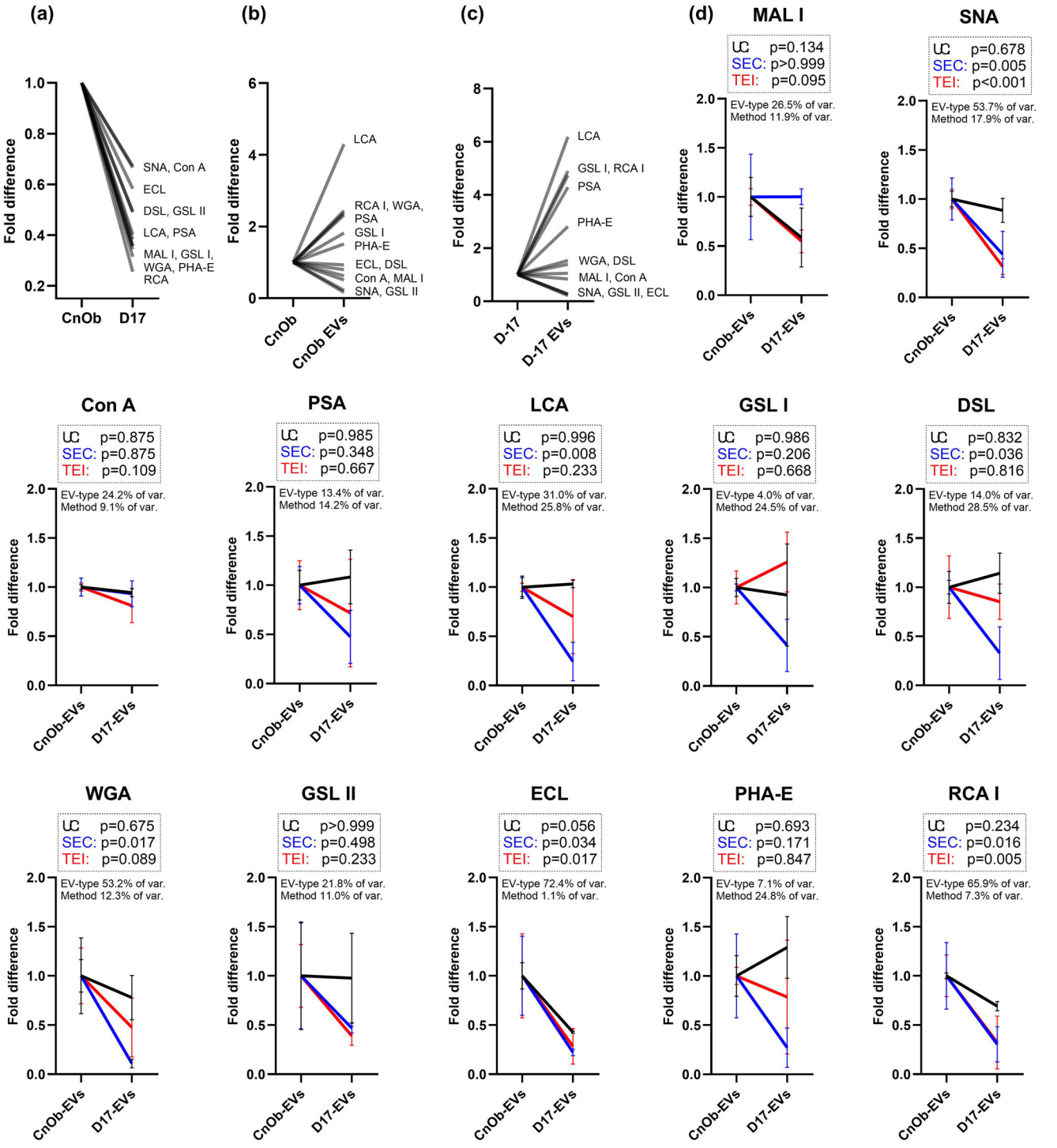


**FIGURE 4** | Comparison of total lane volumes of lectin blots: The adjusted total lane volumes of the lectin blots from Figure 3 were evaluated by the BioRad Image Lab 6.0 software. The mean values of D-17 whole cell lysates were compared to the mean of CnOb cell lysates (=1) and calculated for every lectin separately (a). The mean values of EVs compared to the whole cell lysate (=1) were calculated for every lectin and depicted for CnOb (b) and D-17 (c) to show the relative enrichment of sugars in EVs compared to the producing cell. The values for D-17 EVs of the different separation methods were compared to the mean value of CnOb EVs (=1) for every lectin separately (d), according to the lectin blots in Figure 3, with the aim to depict the alterations of glycosylation in cancer EVs compared to non-cancerous EVs. The *p*-values for every isolation protocol and the influence of the cell of origin and the isolation method as a percentage of the total variance are indicated on the top of every graph.

proteins appear to be successfully removed by SEC, possibly due to the combination with ultrafiltration devices used for sample concentration. It remains unclear whether the removed proteins are merely contaminants or if they contribute to EV functionality as part of a dynamic EV protein corona, which, as suggested by Wolf et al. (2022), may influence EV stability, targeting, and functionality. Considering results of NTA, TEM, and western blot, we conclude that TEI isolates underperform compared to the other isolation methods in terms of purity and reproducibility. This had also been found in connection with EVs from a human gastric cancer line with improved results after previous purification steps like UC and density gradient isolation (Freitas et al. 2019).

Several sugars such as sialic acid, mannose, complex *N*-glycans, were identified earlier to be highly conserved in EVs from different cell lines (Escrevente et al. 2013; Feng et al. 2018). Interestingly, our results for CnOb and OS cells do not match with these reports. MAL I and SNA lectin blots for sialic acid detection showed only moderate signals in the EV isolates compared to the cell lysates, therefore, not indicating a specific enrichment of this sugar in the EV populations.

Moreover, the sialylation in CnOb exceeded sialylation in D-17 cells, which is also in contrast with recent literature reporting that enrichment in terminal sialic acid residues in EV glycosylation is often related with malignancy (Batista et al. 2011; Gomes et al. 2015; Williams et al. 2019). It has been shown that growth factors and cytokines influence cellular glycosylation (Yang et al. 2008). Cell types might react different to cell culture conditions resulting in varying glycoprotein expression and glycosylation patterns. It cannot be excluded, that the higher sialylation of CnOb might be a result of stress by FCS deprivation as reflected by a lower viability of non-tumor cells. As data on glycosylation of canine tumor cells and specially of canine OS are scarce, it is difficult to interpret the sialylation pattern in our OS and CnOb cells. Further studies are necessary to elucidate possible species-specific differences in the glycosylation in these cell types.

The present investigation of EVs revealed enrichment of fucose by LCA and PSA binding, which has been formerly described for microvesicles in a panel of human cells (Batista et al. 2011). *N*-Acetyl-galactosamine (detected by RCA I) and $\alpha$ galactose (GSL I) were also enriched in EVs, which has been reported for EVs from pancreatic cancer cell lines earlier (Matsuda et al. 2020).

The glycosylation pattern rich in complex *N*-linked glycan epitopes (binding to PHA-E) in EVs are in accordance with previous findings where microvesicles showed enrichment in complex *N*-glycan epitopes compared to cell membranes of producing cells (Batista et al. 2011). In our lectin blots, PHA-E binding sugars were highly expressed both in cell lysates and EVs, especially from CnOb cells. This aligns with the glycan composition of EVs from MSCs and osteogenically differentiated MSCs that showed a higher abundance in PHA-E binding in the latter (Shimoda et al. 2019). One of the most characteristic phenotypes of cancer cells is the expression of truncated *O*-glycans due to incomplete synthesis, which are not present in normal cells (Campos et al. 2015). Freitas et al. (2019) could show truncated sialyl Tn (STn) residues to be highly present in the glycoprotein cargo of EVs as demonstrated by anti-STn antibody in a human gastric cancer cell line (MKN45) and a glycoengineered version displaying truncated *O*-glycosylation.

A significant difference between EV separation methods with a loss of cancer-related proteins in EV samples separated by TEI was observed (Freitas et al. 2019). This is in accordance with our findings as we also observed a considerable impact on the detected glycosylation patterns of EV preparations depending on the applied separation method. Interestingly, lectin blots showed similar patterns for UC and TEI preparations with many of our selected lectins. We discovered that SEC enriched CnOb preparations resulted to be higher glycosylated than UC and TEI preparations as the SEC protocol seemingly enriches a divergent EV population, which is especially evident in proteins smaller than 100 kDa. In D-17 EVs, the results are mostly adverse, often with a lower degree of glycosylation after SEC as compared to the other two methods, especially in large proteins. In the work of Freitas et al. (2019) cancer EVs separated by SEC showed more abundant glycosylation compared to UC and TEI, where the pattern of PHA-E binding glycoproteins revealed an additional glycoprotein after SEC and density gradient that was not visible after UC and TEI. In the present work, an additional band after SEC was only detected in CnOb EVs, while the cancer EVs showed less glycosylation after SEC.

A prominent signal at 45 kDa was observed in EV preparations in 10 out of 12 lectin blots. This band was specific for CnOb EVs and predominantly enriched by SEC. It was not detected in the CnOb whole cell lysate and seems therefore highly enriched in EVs. A protein with comparable molecular weight, the A7 antigen, has been described for cells of the osteoblast lineage to recruit osteoclasts (Badawy et al. 2019). Osteoblast factor 45 is another protein of the same size that is highly expressed in osteoblasts (Petersen et al. 2000). This (these) highly glycosylated protein(s) seems to be exclusive for CnOb EVs and warrants further investigation with a proteomic approach.

Tumor cells display a wide range of glycosylation alterations compared with normal cells such as sialylation, fucosylation, *O*-glycan truncation, and *N*- and *O*-linked glycan branching (Pinho and Reis 2015). In our study, lectin blots generally showed a lower degree of glycosylation in EVs from malignant D-17 cells compared to CnOb, which applies also for respective whole cell lysates. Reduced glycosylation may help tumor cell-derived EVs to avoid detection by the immune system. Certain glycan structures are recognized by immune lectins (e.g., sialic acids by siglecs), and their absence or alteration can dampen immune responses (Büll et al. 2014). It has been reported that a lower glycosylation, as often observed in cancer cell-derived EVs, enhances cellular uptake. Deglycosylation with PNGase F and especially with neuraminidase promoted EV uptake by various recipient cells in vitro and suggested a causal relation with the reduction in EV charge (Williams et al. 2019). Neuraminidase-treated EVs from mouse liver cells are more likely to be incorporated in lymph nodes and lungs in vivo as compared to intact EVs (Royo et al. 2019). Uptake of human semen-derived EVs in engineered HeLa cells was increased after desialylation by neuraminidase (Kaddour et al. 2020). Removal of *O*-glycosylation on breast cancer EVs enhanced their uptake by HUVECS (Nishida-Aoki et al. 2020). Adverse results with a positive correlation of EV uptake and sialic acid residues via siglec binding (Shimoda et al.

2017) and a decreased MSC-EV uptake by HUVECs after *N*-deglycosylation by PNGase F treatment (Clos-Sansalvador et al. 2022) have been described. Based on these findings, we deduce that the lower levels of glycosylation in the D-17 EVs might facilitate their uptake, thus supporting metastatic tumor spread as reported for breast cancer cells after *O*-deglycosylation (Nishida-Aoki et al. 2020). However, this assumption needs to be verified by functional in vivo experiments.

Limitations of this study are i) that CnOb reacted more sensitive to serum removal, which might have had an influence on the population and composition of released EVs. ii) We followed the manufacturer´s instructions for separation of EVs from conditioned medium, so we had diverging differential centrifugation protocols for the three separation methods probably biasing the population of isolated EVs. Future studies could overcome these issues by either using EV-depleted FCS, serum alternatives or by decreasing the serum starvation time and by using the exact same differential centrifugation scheme. iii) We used 10% acrylamide mini gels for protein electrophoresis in the lectin blots. Another gel concentration might have been more suitable to depict the differences in glycosylation of the very large proteins.

In conclusion, from a methodological perspective, we observed differences in detected EV protein glycosylation patterns comparing common EV separation methods. Higher analytical reproducibility was observed in EVs enriched by either UC or SEC, along with distinct glycosylation patterns associated with each separation method. Besides, we demonstrated differences in EV number, size and morphology between cell types and an overall reduced glycosylation of EVs from D-17 OS cells compared to CnOb. Further in vitro studies are needed to elucidate how EV separation methods influence EV uptake by host cells and function and which method reflects the "natural" EV components best. Moreover, investigations using EVs isolated from OS patient tumor cells are needed, to better understand the functional impact of EV glycosylation on cellular uptake, downstream signaling, and metastatic behavior.

### Author Contributions

**Ingrid Walter, Daniela Cortes Galvez, Silvio Kau-Strebinger**: conceptualization. **Daniela Cortes Galvez, Silvio Kau-Strebinger**: methodology. **Daniela Cortes Galvez**: data curation. **Daniela Cortes Galvez, Ingrid Walter, Silvio Kau-Strebinger**: writing – original draft preparation. **Daniela Cortes Galvez, Ingrid Walter, Silvio Kau-Strebinger, Simone Gabner**: writing – review and editing. All authors have read and agreed to the published version of the manuscript


### Acknowledgement

We thank Waltraud Tschulenk for the excellent TEM pictures and the related work and Olga Olszanska for her amazing support with laboratory work and blots.

Open Access funding provided by Veterinarmedizinische Universitat Wien/KEMÖ.

### Funding

Open access funding was provided by the University of Veterinary Medicine Vienna and the NTA analysis was realized with the equipment of VetCore Facility, University of Veterinary Medicine Vienna. The authors confirm that no additional funding, grants, or financial support was received for the conduct of this study.


### Ethics Statement

The authors have nothing to report.

### Conflicts of Interest

The authors declare no conflicts of interest.

### Data Availability Statement

The data that support the findings of this study are available from the corresponding author upon reasonable request.

### References


Badawy, T., Y. Kyumoto-Nakamura, N. Uehara, et al. 2019. "Osteoblast Lineage-Specific Cell-Surface Antigen (A7) Regulates Osteoclast Recruitment and Calcification During Bone Remodeling." *Laboratory Investigation* 99, no. 6: 866–884. https://doi.org/10.1038/s41374-018-0179-4.

Batista, B. S., W. S. Eng, K. T. Pilobello, K. D. Hendricks-Muñoz, and L. K. Mahal. 2011. "Identification of a Conserved Glycan Signature for Microvesicles." *Journal of Proteome Research* 10, no. 10: 4624–4633. https://doi.org/10.1021/pr200434y.

Bojar, D., L. Meche, G. Meng, et al. 2022. "A Useful Guide to Lectin Binding: Machine-Learning Directed Annotation of 57 Unique Lectin Specifities." *ACS Chemical Biology* 17, no. 11: 2993–3012. https://doi.org/10.1021/acschembio.1c00689.

Bruland, O. S., H. Hoifodt, G. Saeter, S. Smeland, and O. Fodstad. 2005. "Hematogenous Micrometastases in Osteosarcoma Patients." *Clinical Cancer Research* 11: 4666–4673. https://doi.org/10.1158/1078-0432.CCR-05-0165.

Büll, C., M. H. den Brok, and G. J. Adema. 2014. "Sweet Escape: Sialic Acids in Tumor Immune Evasion." *Biochimica et Biophysica Acta (BBA)—Reviews on Cancer* 1846: 1238–1246. https://doi.org/10.1016/j.bbcan.2014.07.005.

Campos, D., D. Freitas, J. Gomes, and C. Reis. 2015. "Glycoengineered Cell Models for the Characterization of Cancer *O*-Glycoproteome: An Innovative Strategy for Biomarker Discovery." *Expert Review of Proteomics* 12, no. 4: 1–6. https://doi.org/10.1586/14789450.2015.1059758.

Carnino, J. M., K. Ni, and Y. Jin. 2020. "Post-Translational Modification Regulates Formation and Cargo-Loading of Extracellular Vesicles." *Frontiers in Immunology* 11: 948. https://doi.org/10.3389/fimmu.2020.00948.

Chanteloup, G., M. Cordonnier, N. Isambert, et al. 2020. "Monitoring HSP70 Exosomes in Cancer Patients' Follow Up: A Clinical Prospective Pilot Study." *Journal of Extracellular Vesicles* 9, no. 1: 1766192. https://doi.org/10.1080/20013078.2020.1766192.

Choi, J. H., and J. Y. Ro. 2021. "The 2020 WHO Classification of Tumors of Soft Tissue: Selected Changes and New Entities." *Advances in Anatomic Pathology* 28, no. 1: 44–58. https://doi.org/10.1097/PAP.0000000000000284.

Christianson, H. C., K. J. Svensson, T. H. van Kuppevelt, J. Li, and M. Belting. 2013. "Cancer Cell Exosomes Depend on Cell-Surface Heparan Sulfate Proteoglycans for Their Internalization and Functional Activity." *Proceedings of the National Academy of Sciences of USA* 110, no. 43: 17380–17385. https://doi.org/10.1073/pnas.1304266110.

Clos-Sansalvador, M., S. G. Garcia, M. Morón-Font, et al. 2022. "*N*-Glycans in Immortalized Mesenchymal Stromal Cell-Derived Extracellular Vesicles Are Critical for EV–Cell Interaction and Functional Activation of Endothelial Cells." *International Journal of Molecular Sciences* 23, no. 17: 9539. https://doi.org/10.3390/ijms23179539.

Costa- Silva, B., N. M. Aiello, A. J. Ocean, et al. 2015. "Pancreatic Cancer Exosomes Initiate Pre-Metastatic Niche Formation in the Liver." *Nature Cell Biology* 17, no. 6: 816–826. https://doi.org/10.1038/ncb3169.

Di Gregorio, J., L. Di Giuseppe, S. Terreri, et al. 2024. "Protein Stability Regulation in Osteosarcoma: The Ubiquitin-Like Modifications and Glycosylation as Mediators of Tumor Growth and as Targets for Therapy." *Cells* 13, no. 6: 537. https://doi.org/10.3390/cells13060537.

Duan, J., Z. Huang, S. Qin, et al. 2024. "Oxidative stress induces extracellular vesicle release by upregulation of HEXB to facilitate tumour growth in experimental hepatocellular carcinoma." *Journal of Extracellular Vesicles* 13, no. 7: e12468. https://doi.org/10.1002/jev2.12468.

Egenvall, A., A. Nødtvedt, and H. von Euler. 2007. "Bone Tumors in a Population of 400 000 Insured Swedish Dogs up to 10 y of Age: Incidence and Survival." *Canadian Journal of Veterinary Research* 71, no. 4: 292–299.

Escrevente, C., N. Grammel, S. Kandzia, et al. 2013. "Sialogylcoproteins and *N*-Glycans From Secreted Exosomes of Ovarian Carcinoma Cells." *PLoS One* 8, no. 10: e78631. https://doi.org/10.1371/journal.pone.0078631.

Fan, S. J., B. Kroeger, P. P. Marie, et al. 2020. "Glutamine Deprivation Alters the Origin and Function of Cancer Cell Exosomes." *EMBO Journal* 39: e103009. https://doi.org/10.15252/embj.2019103009.

Fan, T. M., and C. Khanna. 2015. "Comparative Aspects of Osteosarcoma Pathogenesis in Humans and Dogs." *Veterinary Sciences* 2, no. 3: 210–230. https://doi.org/10.3390/vetsci2030210.

Feng, Y., Y. Guo, Y. Li, et al. 2018. "Lectin-Mediated in Situ Rolling Circle Amplification on Exosomes for Probing Cancer-Related Glycan Pattern." *Analytica Chimica Acta* 1039: 108–115. https://doi.org/10.1016/j.aca.2018.07.040.

Freitas, D., M. Balmaña, J. Poças, et al. 2019. "Different Isolation Approaches Lead to Diverse Glycosylated Extracellular Vesicle Populations." *Journal of Extracellular Vesicles* 8, no. 1: 1621131. https://doi.org/10.1080/20013078.2019.1621131.

Garcia, N. A., I. Ontoria-Oviedo, H. González-King, A. Diez-Juan, and P. Sepúlveda. 2015. "Glucose Starvation in Cardiomyocytes Enhances Exosome Secretion and Promotes Angiogenesis in Endothelial Cells." *PLoS One* 10, no. 9: e0138849. https://doi.org/10.1371/journal.pone.0138849.

Garimella, R., J. Eskew, P. Bhamidi, et al. 2013. "Biological Characterization of Preclinical Bioluminescent Osteosarcoma Orthotopic Mouse (BOOM) Model: A Multi-Modality Approach." *Journal of Bone Oncology* 2, no. 1: 11–21. https://doi.org/10.1016/j.jbo.2012.12.005.

Gomes, J., P. Gomes-Alves, S. B. Carvalho, et al. 2015. "Extracellular Vesicles From Ovarian Carcinoma Cells Display Specific Glycosignatures." *Biomolecules* 5, no. 3: 1741–1761. https://doi.org/10.3390/biom5031741.

Gong, L., Q. Bao, C. Hu, et al. 2018. "Exosomal miR-675 from metastatic osteosarcoma promotes cell migration and invasion by targeting CALN1." *Biochemical and Biophysical Research Communications* 500, no. 2: 170–176.

Hauser, P., S. Wang, and V. Didenko. 2017. "Apoptotic Bodies: Selective Detection in Extracellular Vesicles." *Methods in Molecular Biology* 1554: 193–200. https://doi.org/10.1007/978-1-4939-6759-9_12.

Hoshino, A., H. S. Kim, L. Bojmar, et al. 2020. "Extracellular Vesicle and Particle Biomarkers Define Multiple Human Cancers." *Cell* 182, no. 4: 1044–1061. https://doi.org/10.1016/j.cell.2020.07.009.

Jacobson, R., S. Ha, S. Tani, et al. 2024. "Differential Extracellular Vesicle Concentration and Their Biomarker Expression of Integrin Av/$\beta$5, EpCAM, and Glypican-1 in Pancreatic Cancer Models." *Scientific Reports* 14, no. 1: 14273. https://doi.org/10.1038/s41598-024-65209-8.

Kaddour, H., T. D. Panzner, J. L. Welch, et al. 2020. "Electrostatic Surface Properties of Blood and Semen Extracellular Vesicles: Implications of Sialylation and HIV-Induced Changes on EV Internalization." *Viruses* 12, no. 10: 117. https://doi.org/10.3390/v12101117.

Kumar, M. A., S. K. Baba, H. Q. Sadida, et al. 2024. "Extracellular vesicles as tools and targets in therapy for diseases." *Signal Transduction and Targeted Therapy* 9, no. 1: 27.

Kao, Y. C., Y. W. Chang, C. P. Lai, et al. 2023. "Ectopic ATP Synthase Stimulates the Secretion of Extracellular Vesicles in Cancer Cells." *Communications Biology* 6: 642. https://doi.org/10.1038/s42003-023-05008-5.

Klein, M. J., and G. P. Siegal. 2006. "Osteosarcoma: Anatomic and Histologic Variants." *American Journal of Clinical Pathology* 125, no. 4: 555–581. https://doi.org/10.1309/UC6K-QHLD-9LV2-KENN.

Liang, Y., W. S. Eng, D. R. Colquhoun, R. R. Dinglasan, D. R. Graham, and L. K. Mahal. 2014. "Complex N-Linked Glycans Serve as a Determinant for Exosome/Microvesicle Cargo Recruitment." *Journal of Biological Chemistry* 289, no. 47: 32526–32537. https://doi.org/10.1074/jbc.M114.606269.

Logozzi, M., D. F. Angelini, A. Giuliani, et al. 2019. "Increased Plasmatic Levels of PSA-Expressing Exosomes Distinguish Prostate Cancer Patients From Benign Prostatic Hyperplasia: A Prospective Study." *Cancers* 11, no. 10: 1149. https://doi.org/10.3390/cancers11101449.

Lorencova, L., T. Bertok, V. Gajdosova, et al. 2020. "Exosomes as a Source of Cancer Biomarkers: Advances in Electrochemical Biosensing of Exosomes." *ChemElectrochem* 7, no. 9: 1956–1973. https://doi.org/10.1002/celc.202000075.

Macklin, R., H. Wang, D. Loo, et al. 2016. "Extracellular Vesicles Secreted by Highly Metastatic Clonal Variants of Osteosarcoma Preferentially Localize to the Lungs and Induce Metastatic Behaviour in Poorly Metastatic Clones." *Oncotarget* 7: 43570–43587. https://doi.org/10.18632/oncotarget.9781.

Mathieu, M., L. Martin-Jaular, G. Lavieu, and C. Théry. 2019. "Specificities of Secretion and Uptake of Exosomes and Other Extracellular Vesicles for Cell-to-Cell Communication." *Nature Cell Biology* 21: 9–17. https://doi.org/10.1038/s41556-018-0250-9.

Matsuda, A., A. Kuno, M. Yoshida, et al. 2020. "Comparative Glycomic Analysis of Exosome Subpopulations Derived From Pancreatic Cancer Cell Lines." *Journal of Proteome Research* 19, no. 6: 2516–2524. https://doi.org/10.1021/acs.jproteome.0c00200.

Mazumdar, A., J. Urdinez, A. Boro, et al. 2020. "Osteosarcoma-Derived Extracellular Vesicles Induce Lung Fibroblast Reprogramming." *International Journal of Molecular Sciences* 21, no. 15: 5451. https://doi.org/10.3390/ijms21155451.

Menck, K., C. Scharf, A. Bleckmann, et al. 2014. "Tumor-derived Microvesicles Mediate Human Breast Cancer Invasion Through Differentially Glycosylated EMMPRIN." *Journal of Molecular Cell Biology* 7, no. 2: 143–153. https://doi.org/10.1093/jmcb/mju047.

Mirabello, L., R. J. Troisi, and S. A. Savage. 2009. "Osteosarcoma Incidence and Survival Rates From 1973 to 2004: Data From the Surveillance, Epidemiology, and End Results Program." *Cancer* 115: 1531–1543. https://doi.org/10.1002/cncr.24121.

Naito, T., K. Jingushi, K. Ueda, and K. Tsujikawa. 2021. "Azurocidin is Loaded Into Small Extracellular Vesicles via its N-linked Glycosylation and Promotes Intravasation of Renal Cell Carcinoma Cells." *FEBS Letters* 595, no. 19: 2522–2532. https://doi.org/10.1002/1873-3468.14183.

Nishida-Aoki, N., N. Tominaga, N. Kosaka, and T. Ochiya. 2020. "Altered Biodistribution of Deglycosylated Extracellular Vesicles Through Enhanced Cellular Uptake." *Journal of Extracellular Vesicles* 9, no. 1: 1713527. https://doi.org/10.1080/20013078.2020.1713527.

Paul, D., A. Paul, D. Mukherjee, et al. 2022. "A Mechanoelastic Glimpse on Hyaluronan-Coated Extracellular Vesicles." *Journal of Physical Chemistry Letters* 13, no. 36: 8564–8572. https://doi.org/10.1021/acs.jpclett.2c01629.

Pinho, S. S., and C. A. Reis. 2015. "Glycosylation in Cancer: Mechanisms and Clinical Implications." *Nature Reviews Cancer* 15, no. 9: 540–555. https://doi.org/10.1038/nrc3982.

Pontis, F., L. Roz, O. Fortunato, and G. Bertolini. 2023. "The Metastatic Niche Formation: Focus on Extracellular Vesicle-Mediated Dialogue Between Lung Cancer Cells and the Microenvironment." *Frontiers in Oncology* 3, no. 13: 1116783. https://doi.org/10.3389/fonc.2023.1116783.

Pinho, S. S., S. Carvalho, J. Cabral, C. A. Reis, and F. Gärtner. 2012. "Canine tumors: A spontaneous animal model of human carcinogenesis." *Translational Research* 159, no. 3: 165–172. https://doi.org/10.1016/j.trsl.2011.11.005.

Petersen, D. N., G. T. Tkalcevic, A. L. Mansolf, R. Rivera-Gonzalez, and T. A. Brown. 2000. "Identification of osteoblast/osteocyte factor 45 (OF45), a bone-specific cDNA encoding an RGD-containing protein that is highly expressed in osteoblasts and osteocytes." *Journal of Biological Chemistry* 275, no. 46: 36172–36180. https://doi.org/10.1074/jbc.M003622200.

Raimondi, L., A. De Luca, A. Gallo, et al. 2020. "Osteosarcoma Cell-Derived Exosomes Affect Tumor Microenvironment by Specific Packaging of microRNAs." *Carcinogenesis* 41, no. 5: 666–677. https://doi.org/10.1093/carcin/bgz130.

Royo, F., U. Cossío, A. Ruiz de Angulo, J. Llop, and J. M. Falcon-Perez. 2019. "Modification of the Glycosylation of Extracellular Vesicles Alters Their Biodistribution in Mice." *Nanoscale* 4: 1531–1537. https://doi.org/10.1039/c8nr03900c.

Shekari, F., F. J. Alibhai, H. Baharvand, et al. 2023. "Cell Culture-Derived Extracellular Vesicles: Considerations for Reporting Cell Culturing Parameters." *Journal of Extracellular Biology* 2, no. 10: e115. https://doi.org/10.1002/jex2.115.

Shimoda, A., S. Sawada, and Y. Sasaki. 2019. "Exosome Surface Glycans Reflect Osteogenic Differentiation of Mesenchymal Stem Cells: Profiling by an Evanescent Field Fluorescence-Assisted Lectin Array System." *Scientific Reports* 9: 11497. https://doi.org/10.1038/s41598-019-47760-x.

Shimoda, A., Y. Tahara, S. Sawada, Y. Sasaki, and K. Akiyoshi. 2017. "Glycan Profiling Analysis Using Evanescent Field Fluorescence Assisted Lectin Array: Importance of Sugar Recognition for Cellular Uptake of Exosomes From Mesenchymal Stem Cells." *Biochemical and Biophysical Research Communications* 491, no. 3: 701–707. https://doi.org/10.1016/j.bbrc.2017.07.126.

Tkach, M., and C. Théry. 2016. "Communication by Extracellular Vesicles: Where We Are and Where We Need to Go." *Cell* 164: 1226–1232. https://doi.org/10.1016/j.cell.2016.01.043.

Valadi, H., K. Ekström, A. Bossios, M. Sjöstrand, J. J. Lee, and J. O. Lötvall. 2007. "Exosome-Mediated Transfer of mRNAs and microRNAs is a Novel Mechanism of Genetic Exchange Between Cells." *Nature Cell Biology* 9: 654–659. https://doi.org/10.1038/ncb1596.

EV-TRACK Consortium. Van Deun, J., P. Mestdagh, et al. 2017. "EV-TRACK: Transparent Reporting and Centralizing Knowledge in Extracellular Vesicle Research." *Nature Methods* 14: 228–232. https://doi.org/10.1038/nmeth.4185.

van Niel, G., G. D'Angelo, and G. Raposo. 2018. "Shedding Light on the Cell Biology of Extracellular Vesicles." *Nature Reviews Molecular Cell Biology* 19, no. 4: 213–217. https://doi.org/10.1038/nrm.2017.125.

Wang, Z., X. Sun, A. Natalia, et al. 2020. "Dual Selective Magnetic Analysis of Extracellular Vesicle Glycans." *Matter* 2, no. 1: 150–166. https://doi.org/10.1016/j.matt.2019.10.018.

Welsh, J. A., D. C. I. Goberdhan, L. O'Driscoll, et al. 2024. "Minimal Information for Studies of Extracellular Vesicles (MISEV2023): From Basic to Advanced Approaches." *Journal of Extracellular Vesicles* 13, no. 2: e12404. https://doi.org/10.1002/jev2.12416.

Williams, C., R. Pazos, F. Royo, et al. 2019. "Assessing the Role of Surface Glycans of Extracellular Vesicles on Cellular Uptake." *Scientific Reports* 9: 11920. https://doi.org/10.1038/s41598-019-48499-1.

Wolf, M., R. W. Poupardin, P. Ebner-Peking, et al. 2022. "A Functional Corona Around Extracellular Vesicles Enhances Angiogenesis, Skin Regeneration and Immunomodulation." *Journal of Extracellular Vesicles* 11, no. 4: e12207. https://doi.org/10.1002/jev2.12207.

Yang, X., J. Yip, M. Harrison, and I. Brockhausen. 2008. "Primary Human Osteoblasts and Bone Cancer Cells as Models to Study Glycodynamics in Bone." *International Journal of Biochemistry & Cell Biology* 40, no. 3: 471–483. https://doi.org/10.1016/j.biocel.2007.08.009.

Zhang, J., Y. Qin, Q. Jiang, et al. 2022. "Glycopattern Alteration of Glycoproteins in Gastrointestinal Cancer Cell Lines and Their Cell-Derived Exosomes." *Journal of Proteome Research* 21, no. 8: 1876–1893. https://doi.org/10.1021/acs.jproteome.2c00159.

Zhongyu, X., X. Wei, Z. Hongmei, et al. 2024. "Review of Pre-Metastatic Niches Induced by Osteosarcoma-Derived Extracellular Vesicles in Lung Metastasis: A Potential Opportunity for Diagnosis and Intervention." *Biomedicine and Pharmacotherapy* 178: 117203. https://doi.org/10.1016/j.biopha.2024.117203.

## Supporting Information

Additional supporting information can be found online in the Supporting Information section.

**Supplementary Figure**: jex270119-sup-001-SupMat.jpg